Linearized Inversion of Reflection Traveltimes

U.S. GEOLOGICAL SURVEY BULLETIN 1965

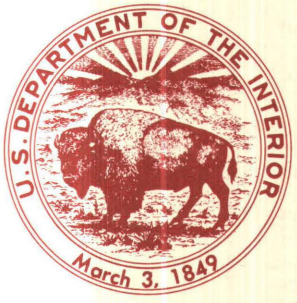

AVAILABILITY OF BOOKS AND MAPS OF THE U.S. GEOLOGICAL SURVEY

Instructions on ordering publications of the U.S. Geological Survey, along with prices of the last offerings, are given in the current-year issues of the monthly catalog "New Publications of the U.S. Geological Survey." Prices of available U.S. Geological Survey publications released prior to the current year are listed in the most recent annual "Price and Availability List." Publications that are listed in various U.S. Geological Survey catalogs (**see back inside cover**) but not listed in the most recent annual "Price and Availability List" are no longer available.

Prices of reports released to the open files are given in the listing "U.S. Geological Survey Open-File Reports," updated monthly, which is for sale in microfiche from the U.S. Geological Survey, Books and Open-File Reports Section, Federal Center, Box 25425, Denver, CO 80225. Reports released through the NTIS may be obtained by writing to the National Technical Information Service, U.S. Department of Commerce, Springfield, VA 22161; please include NTIS report number with inquiry.

Order U.S. Geological Survey publications **by mail** or **over the counter** from the offices given below.

BY MAIL

Books

Professional Papers, Bulletins, Water-Supply Papers, Techniques of Water-Resources Investigations, Circulars, publications of general interest (such as leaflets, pamphlets, booklets), single copies of Earthquakes & Volcanoes, Preliminary Determination of Epicenters, and some miscellaneous reports, including some of the foregoing series that have gone out of print at the Superintendent of Documents, are obtainable by mail from

U.S. Geological Survey, Books and Open-File Reports
Federal Center, Box 25425
Denver, CO 80225

Subscriptions to periodicals (Earthquakes & Volcanoes and Preliminary Determination of Epicenters) can be obtained ONLY from the

Superintendent of Documents
Government Printing Office
Washington, D.C. 20402

(Check or money order must be payable to Superintendent of Documents.)

Maps

For maps, address mail orders to

U.S. Geological Survey, Map Distribution
Federal Center, Box 25286
Denver, CO 80225

Residents of Alaska may order maps from

Alaska Distribution Section, U.S. Geological Survey,
New Federal Building - Box 12
101 Twelfth Ave., Fairbanks, AK 99701

OVER THE COUNTER

Books

Books of the U.S. Geological Survey are available over the counter at the following Geological Survey Public Inquiries Offices, all of which are authorized agents of the Superintendent of Documents:

- **WASHINGTON, D.C.**--Main Interior Bldg., 2600 corridor, 18th and C Sts., NW.
- **DENVER, Colorado**--Federal Bldg., Rm. 169, 1961 Stout St.
- **LOS ANGELES, California**--Federal Bldg., Rm. 7638, 300 N. Los Angeles St.
- **MENLO PARK, California**--Bldg. 3 (Stop 533), Rm. 3128, 345 Middlefield Rd.
- **RESTON, Virginia**--503 National Center, Rm. 1C402, 12201 Sunrise Valley Dr.
- **SALT LAKE CITY, Utah**--Federal Bldg., Rm. 8105, 125 South State St.
- **SAN FRANCISCO, California**--Customhouse, Rm. 504, 555 Battery St.
- **SPOKANE, Washington**--U.S. Courthouse, Rm. 678, West 920 Riverside Ave..
- **ANCHORAGE, Alaska**--Rm. 101, 4230 University Dr.
- **ANCHORAGE, Alaska**--Federal Bldg, Rm. E-146, 701 C St.

Maps

Maps may be purchased over the counter at the U.S. Geological Survey offices where books are sold (all addresses in above list) and at the following Geological Survey offices:

- **ROLLA, Missouri**--1400 Independence Rd.
- **DENVER, Colorado**--Map Distribution, Bldg. 810, Federal Center
- **FAIRBANKS, Alaska**--New Federal Bldg., 101 Twelfth Ave.

Linearized Inversion of Reflection Traveltimes

By MYUNG W. LEE and
WARREN F. AGENA

U.S. GEOLOGICAL SURVEY BULLETIN 1965

U.S. DEPARTMENT OF THE INTERIOR
MANUEL LUJAN, JR., Secretary

U.S. GEOLOGICAL SURVEY
Dallas L. Peck, Director

UNITED STATES GOVERNMENT PRINTING OFFICE: 1991

For sale by the
Books and Open-File Reports Section
U.S. Geological Survey
Federal Center
Box 25425
Denver, CO 80225

Library of Congress Cataloging-in-Publication Data

Lee, Myung W.
Linearized inversion of reflection traveltimes / by Myung W. Lee and Warren F. Agena.
p. cm. — (U.S. Geological Survey bulletin ; 1965)
Includes bibliographical references.
1. Seismic traveltime inversion. 2. Seismic reflection method. 3. Seismology—Mathematical models. I. Agena, Warren F. II. Title. III. Series.
QE75.B9 no. 1965
[QE539.2.S43]
557.3 s—dc20 91-7790
[551.2'2] CIP

CONTENTS

FIGURES

TABLES

Linearized Inversion of Reflection Traveltimes

By Myung W. Lee *and* Warren F. Agena

Abstract

A computationally accurate and efficient traveltime inversion method for a plane-layered earth model can be formulated using a generalized linear-inversion technique. Suitable parameterization enables us to estimate layer variables such as velocity, dip, and depth simultaneously for all layers by iteratively solving the reduced-size matrix.

Although computationally similar to the layer-stripping method, our method offers advantages in terms of convergence and consistency of the traveltime inversion.

This method was applied both in the shot and common midpoint (CMP) domains, and results indicate that the shot domain inversion is more sensitive to measurement noise compared to the CMP domain inversion. We used a regularization method to overcome the adverse effects of measurement noise, but the method often resulted in inconsistent parameter estimation. This suggests that care must be taken when implementing regularization.

The formulas presented are also applicable to the traveltime inversion of mode-converted waves when longitudinal- or shear-wave velocity is known.

INTRODUCTION

An accurate estimation of interval velocities and reflector geometry enables us to perform detailed geological analysis of seismic data. Interval velocities are extremely important in constraining lithologic interpretations of deep crustal seismic data. Conventional velocity estimation in reflection seismology is performed in the common midpoint (CMP) domain under the assumption of hyperbolic moveout and negligible dip angle. This method works well when offset distance is small compared to target depth and when reflections have moderate dips. In order to overcome these limitations, a linearized inversion method in both the CMP domain and shot domain is presented in this paper.

Traveltime inversion is one of many non-linear geophysical inversion problems and has been applied for a long time to observed earthquake data in order to investigate the internal structure of the earth (Aki and Richards, 1980). Generalized linear-inversion theory has also been used to solve the non-linear traveltime inversion problem (Backus and Gilbert, 1970; Aki and Lee, 1976). Aki and Richards (1980), Tarantola (1987), and Lines (1988) have written papers that contain excellent discussions of generalized inversion theory. Lines (1988) also compiled significant recent papers related to geophysical inverse problems.

Traveltime inversion can be formulated either in a distance-time (x-t) domain or in an intercept time-horizontal slowness (τ-p) domain. Diebold and Stoffa (1981) developed a τ-p traveltime inversion method valid for both reflections and refractions and Diebold and others (1988) applied this method to expanding-spread profile (ESP) data with offsets of 6.5 to 14 km. Diebold and others (1988) analyzed wide angle reflection and refraction data and computed interval velocities for intervals as deep as 30 km in the area of the Baltimore Canyon trough on the east coast of the United States.

Liu and others (1986) applied the x-t domain inversion method to ESP data acquired in the Sevier desert of west-central Utah and estimated interval velocities in intervals as deep as 30 km.

Inversion of reflection times in three dimensions using surface seismic data was discussed by Gjøystdal and Ursin (1981). They estimated interval velocities and reflection interfaces using a layer-stripping method. Bishop and others (1985) applied a tomographic inversion technique in order to estimate interval velocity and reflector depth in a laterally varying medium using surface seismic profiles. A tomographic inversion technique to obtain two- and three-dimensional velocity structures of the subsurface using well logs, vertical seismic profiles (VSP's), and surface measurements was investigated by Chiu and Stewart (1987). They also extended the inversion method to transversely isotropic media.

In this paper, a traveltime inversion method in the x-t domain is formulated by suitable parameterization and by explicit expression of the Jacobian matrix. The formula was developed assuming iso-velocity layers separated by plane boundaries within the earth's crust. This paper posits that the general inverse problem of simultaneously estimating

Manuscript approved for publication November 30, 1990.

layer parameters is equivalent to iteratively computing the reduced-size matrix. This method is computationally similar to the layer-stripping method. In the case of a model with N layers containing M observations for each layer, conventional simultaneous parameter estimation involves the inversion of a $3N \times NM$ matrix, whereas our method involves the inversion of a $3 \times M$ matrix N times. By introducing explicit derivatives and suitable parameterization, the inversion method becomes computationally efficient and accurate.

The method is suitable to the traveltime inversion of surface shot or CMP gathers and can easily accommodate the inversion of mode-converted waves. We tested the method on real marine and land multichannel seismic data to determine its feasibility and limitations. Traveltime inversion in terms of the domain of application, field configuration, resolution, and regularization are also discussed.

ACKNOWLEDGMENTS

We thank John J. Miller and William A. Schneider, Jr. for their constructive reviews.

THEORY

Many researchers have extensively investigated the application of linear inverse theory to traveltime inversion and other geophysical problems. Theoretical development for geophysical inversion has been intensive (Aki and Richards, 1980; Tarantola, 1987; Lines and Treitel, 1984). The details of traveltime inversion using the generalized inverse are given by Lee (1990). Thus, only brief discussion of theory pertinent to the understanding of this paper is given.

The solution of nonlinear inverse problems generally begins with a Taylor series expansion of the computed model response for a given parameter distribution. Parameters are updated iteratively assuming convergence to a global minimum. Thus, traveltime can be approximated by the following series expansion that retains only the first order terms:

$$t_N(\boldsymbol{P}^{n+1}) \approx t_N(\boldsymbol{P}^n) + \sum_{j=1}^{L} \left(\frac{\partial t_N}{\partial P_j}\right)_{\boldsymbol{P}=\boldsymbol{P}^n} \delta P_j \quad (1)$$

where

t_N is the traveltime from the Nth reflector with dimension M,

$\boldsymbol{P}^{n+1}$ is the $(n+1)$th estimation of parameters with dimension L, and

δP_j is the parameter update given by:

$$\delta P_j = P_j^{n+1} - P_j^n$$

The least squares solution of δP_j in equation 1 for a given observation O_i (i=1, 2, ..., M) is attained by minimizing the mean-squared error (E):

$$E = \sum_{i=1}^{M} \left[O_i - t_i(\boldsymbol{P}^{n+1}) \right]^2$$

$$= \sum_{i=1}^{M} \left[O_i - t_i(\boldsymbol{P}^n) - \sum_{j=1}^{L} \left(\frac{\partial t_i}{\partial P_j}\right)_{\boldsymbol{P}=\boldsymbol{P}^n} \delta P_j \right]^2 \quad (2)$$

The formal solution of equation 2, as given by the least squares method, can be written as:

$$\delta \boldsymbol{P} = \boldsymbol{G}^{-1}(\boldsymbol{O} - \boldsymbol{t}^n) = \boldsymbol{G}^{-1}\ \delta \boldsymbol{m} \quad (3)$$

where

$\boldsymbol{G}^{-1}$ is the generalized inverse of the $M \times L$ Jacobian matrix,

$\boldsymbol{O}$ is the M-dimensional column vector of the observations,

$\boldsymbol{t}^n$ is the M-dimensional column vector of the modeled traveltime at the nth iteration, and

$\boldsymbol{P}$ is the L-dimensional column vector of layer parameters.

The conventional matrix inverse ($\boldsymbol{G}^{-1}$) exists only if $\boldsymbol{G}$ is square ($M = L$) and nonsingular. However, $M >> L$ for most inverse problems, so the matrix inverse presented in this paper is identified with the general inverse case (see, e.g., Aki and Richards, 1980, chapter 12). As shown in equations 2 and 3, the essence of traveltime inversion is the evaluation of the Jacobian matrix and its generalized inverse. Using the singular value decomposition method for the generalized inverse, the solution of equation 3 can be written as:

$$\boldsymbol{P}^{n+1} = \boldsymbol{P}^n + \boldsymbol{V}\Lambda^{-1}\boldsymbol{U}^T(\boldsymbol{O} - \boldsymbol{t}^n) \quad (4)$$

where

V is an $L \times L$ matrix of orthonormal eigenvectors,

U is an $M \times M$ matrix of orthonormal eigenvectors, and

Λ is a diagonal matrix of L singular values.

It is apparent from equation 3 that accurate estimation of the Jacobian matrix is important in order to solve nonlinear inversion problems. Generally, a finite difference approximation can be used for the evaluation of the Jacobian matrix (Lines and others, 1984). In order to increase the accuracy and speed of the computation for the layered-earth model, an explicit expression of the Jacobian matrix is derived here.

Figure 1 shows a simple ray-path diagram for the derivation of the Jacobian matrix including mode conversion. We define the coordinate of the intersection of the downgoing ray with ith interface as (X_i, Z_i) and for the upgoing ray as $(\tilde{X}_i, \tilde{Z}_i)$. The traveltime from the source to the kth receiver via the reflection at the Nth interface (T^k) can

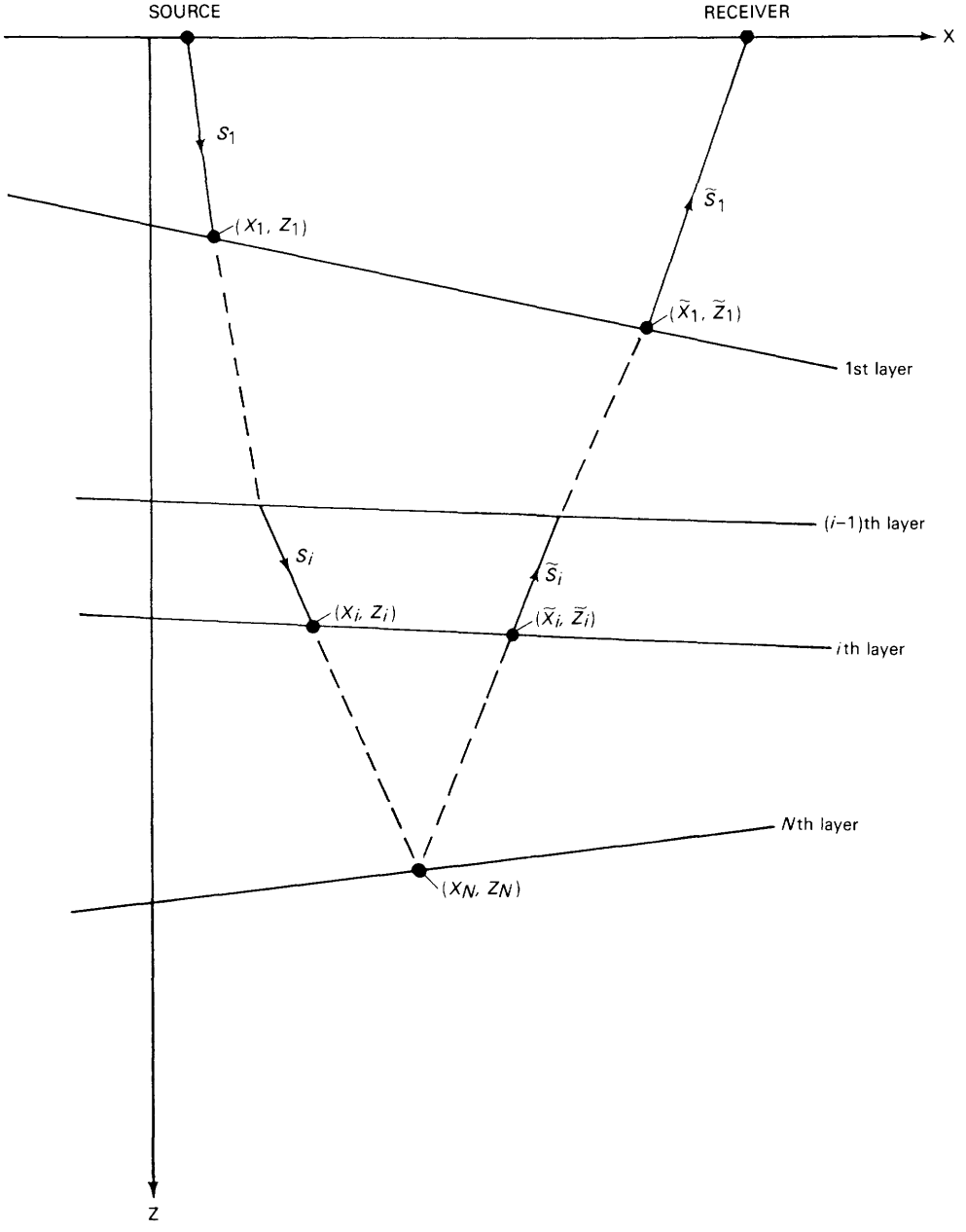

Figure 1. Schematic ray-path diagram for a reflection from the Nth interface. (X_i, Z_i) represents the intersection of a downgoing wave with the layer interface; $(\tilde{X}_i, \tilde{Z}_i)$ represents the intersection for upgoing waves. S_i is the slowness of the downgoing wave and $\tilde{S}_i$ is the slowness of the upgoing wave.

be written by:

$$T_N^k = \sum_{i=1}^{N} \left[s_i Q_{N,i}^k + \tilde{s}_i \tilde{Q}_{N,i}^k \right] = \sum_{i=1}^{N} s_i Q_{N,i}^k + U \quad (5)$$

where

s_i is the slowness of the downgoing wave in ith medium,

$\tilde{s}_i$ is the slowness of the upgoing wave in the ith medium, and

$$Q_{N,i}^k = \left((\Delta X_{N,i}^k)^2 + (\Delta Z_{N,i}^k)^2 \right)^{1/2}$$

$$\Delta X_{N,i}^k = X_{N,i}^k - X_{N,i-1}^k$$

$$\Delta Z_{N,i}^k = Z_{N,i}^k - Z_{N,i-1}^k$$

The tilde indicates a quantity corresponding to the upgoing ray path and is denoted as "U" from here on for notational simplicity. As indicated in equation 5, if there is no mode conversion at the reflecting boundary, $\tilde{s}_i = s_i$.

As shown in equation 5, $Q_{N,i}^k$ represents the length of ray segment between (i–1)th and ith interface (or medium i) for the ray reflected from the Nth interface and received at the kth geophone. The dipping layer is defined using slope a_i and intercept h_i by:

$$Z_i = a_i X_i + h_i$$

Thus, $Z_{N,i}^k$ can be written as:

$$Z_{N,i}^k = a_i X_{N,i}^k + h_i \quad (6)$$

Using the above notation, the required derivatives shown in equation 2 may be written as follows:

$$\frac{\partial T_N^k}{\partial s_j} = Q_{N,j}^k$$

$$\frac{\partial T_N^k}{\partial \tilde{s}_j} = \tilde{Q}_{N,j}^k$$

$$\frac{\partial T_N^k}{\partial a_j} = s_j (Q_{N,j}^k)^{-1} \Delta Z_{N,j}^k X_{N,j}^k - \quad (7)$$

$$s_{j+1} (Q_{N,j+1}^k)^{-1} \Delta Z_{N,j+1}^k X_{N,j+1}^k + U$$

$$\frac{\partial T_N^k}{\partial h_j} = s_j (Q_{N,j}^k)^{-1} \Delta Z_{N,j}^k - s_j (Q_{N,j}^k)^{-1} \Delta Z_{N,j+1}^k + U$$

In all cases in equation 7, $j \le N$. A similar derivation of the derivatives of traveltime with respect to layer parameters without mode conversion is given by Lee (1990).

COMPUTATIONAL ASPECT

If we assume N reflections measured with M geophones and no mode conversion at the reflecting boundary, then equation 3 can be written in the following matrix form:

$$\begin{bmatrix} G_{11} & & & \\ G_{12} & G_{22} & & \\ \vdots & \vdots & & \\ G_{1N} & G_{2N} & \cdots & G_{NN} \end{bmatrix} \begin{bmatrix} \delta P_1 \\ \delta P_2 \\ \vdots \\ \delta P_N \end{bmatrix} = \begin{bmatrix} \delta m_1 \\ \delta m_2 \\ \vdots \\ \delta m_N \end{bmatrix} \quad (8)$$

where

δP_i is the ith layer parameter update defined as a column vector of (δs_i, δa_i, δh_i), and

δm_i is a column vector of order M consisting of the difference between observed and computed arrival times from the ith layer.

In equation 8, the matrix elements $G_{i\,j}$ are themselves matrices defined as:

$$G_{ij} = \begin{bmatrix} \frac{\partial T_j^1}{\partial s_i} & \frac{\partial T_j^1}{\partial a_i} & \frac{\partial T_j^1}{\partial h_i} \\ \vdots & \vdots & \vdots \\ \frac{\partial T_j^M}{\partial s_i} & \frac{\partial T_j^M}{\partial a_i} & \frac{\partial T_j^M}{\partial h_i} \end{bmatrix}$$

As indicated above, the matrix elements of $G_{i\,j}$ consist of the derivatives of the traveltime reflected from the jth interface with respect to the ith model parameters. By defining the parameter vector as shown in equation 8, the generalized inverse of equation 8 can be computed easily because matrix G is in a lower triangular form. The iterative solution of the general inverse is given as follows:

$$\delta \boldsymbol{P}_1 = (\boldsymbol{G}_{11})^{-1}\ \delta \boldsymbol{m}_1$$

$$\delta \boldsymbol{P}_2 = (\boldsymbol{G}_{22})^{-1}\ (\delta \boldsymbol{m}_2 - \boldsymbol{G}_{12}\delta \boldsymbol{P}_1) \qquad (9)$$

.

.

.

$$\delta \boldsymbol{P}_N = (\boldsymbol{G}_{NN})^{-1}\ \left(\delta \boldsymbol{m}_N - \sum_{i=1}^{N-1}\ \boldsymbol{G}_{iN}\,\delta \boldsymbol{P}_i\right)$$

Thus, instead of solving the $3N \times MN$ matrix shown in equation 8, this arrangement of parameters leads to the inverse of a $3 \times M$ matrix N times. This reduced matrix dimension reduces computation time and increases the numerical accuracy of the matrix inversion. We call this method the iterative whole-layer inversion (IWI) method. The layer-stripping method used by Lines and others (1984) is very similar to this approach from a computational point of view. The main advantages of the IWI method are:

1. Computationally, it is equivalent to the layer-stripping method. The only computational overhead is the additional matrix multiplication, shown in equation 9.
2. Unlike the layer-stripping method, the errors of the upper layers do not propagate to the lower layers.
3. In the case of high noise contamination with a poor initial estimate, the IWI method converges to the expected solution better than the layer-stripping method. This will be shown later in the model study.
4. Because it involves a reduced size matrix, numerical accuracy and computational efficiency can be achieved.

Some disadvantages of this approach compared to the layer-stripping technique are the slow convergence for a poorly defined initial estimate and more cross talk between parameters in an unconstrained problem.

In practice, we do not use equation 9 directly because the iteration may not converge due to the non-linearity of the inverse problem. To circumvent this problem, we use a formula from Aki and Richards (1980):

$$\delta \boldsymbol{P} = \beta\, \boldsymbol{G}^{-1}\, \delta \boldsymbol{m} \qquad (10)$$

where

$0 < \beta \leq 1$.

Numerical simulation indicates that β is a very important parameter when the initial estimate is poor. A suitable choice for β improves the result of inversion and will be discussed later.

COMPARISON OF METHODS

In the previous section, we briefly discussed the advantage of the IWI method over the layer-stripping method. In this section, the performance of the IWI method will be examined through numerical simulations (models).

Table 1 shows the layer parameters used for model 1 and the parameters for the initial estimate. The ray-path diagram for a shot gather with 0.2 km group intervals and a split-spread geometry is shown in figure 2*A*. The ray path for the initial estimate is shown in figure 2*B*. As can be seen from figure 2, the initial estimate is poorly defined for this model. The initial root-mean-square (RMS) error between the arrival times of the model and the initial estimate was 1.757 s. Generalized inversion using the IWI method reduced the RMS error to the expected numerical accuracy of 3×10^{-5} s in seven iterations. The layer-stripping method also produced the same result.

In the case of low noise contamination, where travel-time data were contaminated with Gaussian random noise having a standard deviation of less than 8 ms ($\sigma_t < 8$ ms), both methods converged to similar numerical values. In the case of high noise contamination ($\sigma_t = 16$ ms), inversion results from both methods were quite different for certain layers even though both methods converged to the expected RMS error. Inversion results with $\sigma_t = 16$ ms are shown in table 2. Notice the differences in parameters for layer 4. The layer-stripping method provided a much lower interval velocity of 2.42 km/s compared with the true velocity of 4.8 km/s and calculated a thickness of 30 m instead of the true value of 100 m. The inversion result from the IWI method produced an interval velocity of 4.86 km/s and a layer thickness of 100 m. Except for this discrepancy, inversion results from both methods are quite similar.

With slightly different initial conditions, the layer-stripping method converged to different numerical values in many cases, but the IWI method converged to consistent numerical values in most of the cases we tried. For example, with $\beta = 0.5$ in equation 10 (instead of $\beta = 0.42$, which was used for the result shown in table 2), the inversion results by the layer-stripping method were very similar to those determined by the IWI method shown in table 2.

In order to examine the effects of β on convergence to a solution and to test the consistency of the solution, the IWI method was applied to the model shown in figure 2*A*. The RMS error, with respect to iteration number and β, for $\sigma_t = 16$ ms is shown in figure 3. The computer program initializes β to 1.0, and, in succeeding iterations, if the RMS error is larger than the error of the previous iteration, β is adjusted in order to prevent divergence. Figure 3 shows an increase in RMS error from iteration 1 to 2. Thus, β was adjusted to the values shown in figure 3 to allow convergence.

Figure 3 indicates that if β is too large or too small ($\beta = 0.2$ or $\beta = 1.0$), the IWI method does not converge to the

Table 1. Layer parameters for model 1 and initial estimate for traveltime inversion

Layer number	Velocity (kilometers per second) P-wave	Velocity (kilometers per second) S-wave	Dip (degrees)	Depth (kilometers)
Model 1 parameters				
1	1.5	1.0	7.0	0.7
2	2.5	1.25	-5.0	1.3
3	3.8	1.9	0.0	2.0
4	4.8	2.5	0.0	2.1
5	3.8	2.0	-10.0	3.0
6	4.2	1.9	15.0	5.0
7	3.5	1.6	0.0	7.0
Initial estimate for P–P reflection inversion				
1	1.5		0.0	0.3
2	2.0		0.0	2.0
3	2.5		0.0	3.8
4	3.0		0.0	5.0
5	3.5		0.0	6.0
6	4.0		0.0	6.5
7	4.0		0.0	7.0

solution. Also, the converged solution indicates consistent estimates of layer parameters. This figure also shows that the rate of convergence depends on the value of β. For example, the IWI method converged in five iterations for $\beta = 0.6$, but in seven iterations for $\beta = 0.8$. There seems to be an optimum value of β for a given problem, but currently we do not know how to choose the optimum value at each iteration.

The consistent numerical results achieved by the IWI method indicate a distinct advantage over results obtained by the layer-stripping method. This example demonstrates the flexibility of the IWI method in choosing the β parameter.

ACCURACY OF INVERSION

The accuracy of traveltime inversion depends primarily on the error in observation in relation to the shooting geometry. Numerical simulations using the model parameters shown in table 1 indicate that, for the noise-free case, the inversion converged to the true layer parameters even though the length of surface spread (L) was much smaller than the target depth (h). For example, using the initial estimates shown in table 1, the traveltime data with a 0.05 km group interval and 20 channels converged to the true solution (this corresponds to $L/h \approx 0.15$ for the deepest target). However, with a small error in the observation (σ_t = 2 ms), the inversion result showed a large deviation from the exact layer parameters even though it converged to the expected accuracy (RMS error $\approx$ 1.8 ms). The velocity, dip, and depth of layer 7 were calculated to be 3.18 km/s, –22.71°, and 10.22 km when σ_t = 2 ms.

The quantitative aspect of inversion error due to errors in observation can be analyzed using equation 3. Let us assume that there is no measurement error and the inversion converged to the solution in the nth iteration. Then, $(\delta \boldsymbol{P})_n = (\boldsymbol{G}^{-1})_n\, (\delta \boldsymbol{m})_n \approx 0$, since $\delta \boldsymbol{m}$ (the difference between observed and computed arrival times) is zero. But, if there is uncorrelated Gaussian random measurement error, the variance of the model parameters can be written as:

$$\text{Var}\,(\delta \boldsymbol{P}) = \text{Var}\,(\boldsymbol{G}^{-1}\,\delta \boldsymbol{m})$$

$$= (\boldsymbol{G}^{-1})^T\,(\boldsymbol{G}^{-1})\,(\sigma_t)^2$$

where

Var represents the variance, and

σ_t represents the standard deviation of the measurement error.

The variance, from equation (4) and Jackson (1972), can be written as:

$$\text{Var}\,(\delta \boldsymbol{P}) = \Sigma\, V_{ij}^2 \left(\frac{\sigma_t}{\lambda_j}\right)^2 \qquad (11)$$

where

λ_j are the singular values of the Jacobian Matrix $\boldsymbol{G}$, and

V_{ij} are the orthonormal eigenvectors.

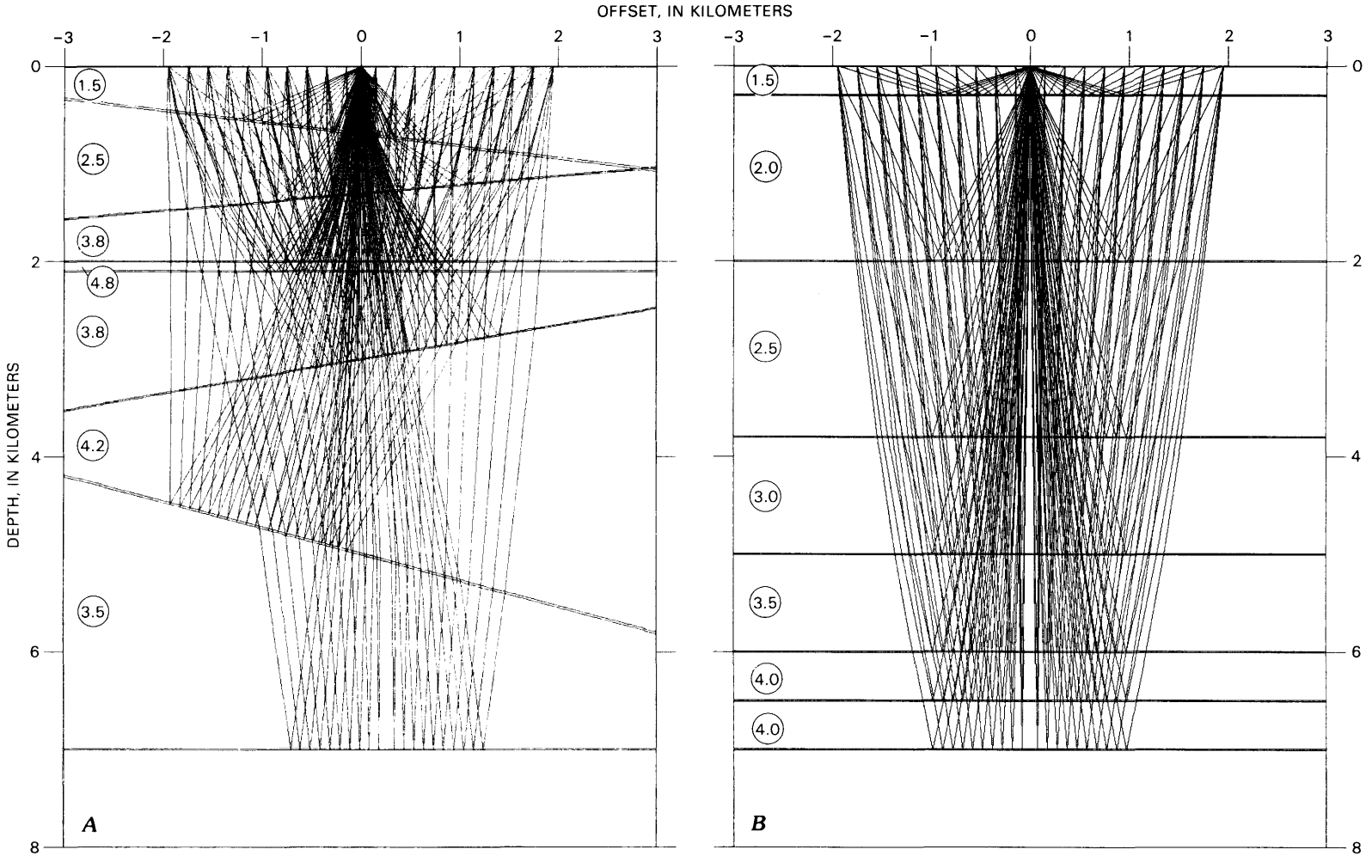

Figure 2. Ray tracings for a split-spread shot gather for the shot domain inversion test. The geophone group interval is 0.2 km and near-offset distance is 0.1 km. P-wave velocities for each layer (in km/s), from table 1, are circled. *A*, Model whose parameters are shown in table 1; *B*, Initial estimate whose parameters are shown in table 1.

Table 2. Inversion results using split-spread shooting geometry

[Shooting geometry shown in figure 2. Random noise content (σ_t) equals 16 milliseconds; group interval equals 200 meters; near-offset distance equals 152 meters; 20 channels]

Layer number	Velocity (kilometers per second) P-wave	Dip (degrees)	Depth (kilometers)
Layer-stripping method			
1	1.53	7.46	0.72
2	2.52	-4.79	1.31
3	3.96	-0.12	2.05
4	2.42	0.58	2.08
5	3.70	-10.35	2.97
6	4.50	17.52	5.14
7	6.90	-14.00	9.19
Iterative whole-layer conversion method (IWI)			
1	1.53	7.46	0.72
2	2.52	-4.79	1.31
3	3.96	-0.12	2.04
4	4.86	1.44	2.14
5	3.46	-8.71	2.95
6	4.46	18.85	5.13
7	6.93	-13.01	9.13

Detailed derivation and discussions on measurement error may be found in van der Sluis and van der Vorst (1987).

Equation 11 indicates that the error of the layer parameters depends on the singular values of the Jacobian matrix: as λ_j becomes smaller, the effect on the accuracy becomes more pronounced.

In order to get some insight into inversion accuracy in relation to the singular values, a simple one-layered model with velocity (v) = 2 km/s, dip (ϕ) = 20°, and target depth (h) = 2 km was used. The smallest singular value (λ_s) for this model with various L/h ratios is shown in figure 4. When L/h is equal to 1, $\lambda_s \approx 0.04$. When L/h is less than 1, λ_s decreases very rapidly with respect to decreasing L/h. When L/h is greater than 1, the variation of λ_s with respect to the increasing L/h is flattened out. Thus, the inversion result of the previous example with 0.05 km group intervals could have a large uncertainty for the deepest layer where $L/h \approx 0.15$.

The smallest singular values (λ_s) for the single-layer model considered previously (v = 1 km/s) are indicated in figure 4 as squares at L/h=1 and L/h = 2; λ_s values for v = 4 km/s are indicated as crosses. The general trend for v = 1 km/s or v = 4 km/s is very similar to that of v = 2 km/s. The smallest singular value for the higher interval velocity is less than that for the lower interval velocity. This figure implies that the inversion results for smaller interval velocities have less variance than those for large interval velocities with the same measurement error. The analysis of singular values for different models leads us to conclude that the key factor controlling the accuracy of inversion is the arrival time difference between near- and far-offset distance.

Table 3 shows a series of inversion results for model 1 (table 1, fig. 1) with respect to variable amounts of noise contamination. When $\sigma_t < 8$ ms, errors of inversion for the upper five layers are less than about 5 percent. The L/h ratio for the fifth layer is about 1.3, so L/h values for the upper five layers are greater than 1. Thus, the variances of layer parameters for the upper five layers are small and the inversion results are reliable. The results shown in table 3 demonstrate the increasing error with respect to increasing measurement error and increasing depth. The largest error occurs for layer 7. In this case, even for a small error of σ_t = 4 ms, the velocity error is about 20 percent.

In any inversion problem, very small singular values have a dramatic effect on the solution. In order to circumvent this problem, a regularization is sometimes employed in the inversion process. In the singular value decomposition method, regularization can be implemented by dropping the solutions corresponding to small singular values (van der Sluis and van der Vorst, 1987), but this introduces another kind of error called regularization error. As mentioned by van der Sluis and van der Vorst (1987), regularization reduces the variance of the solution but gives

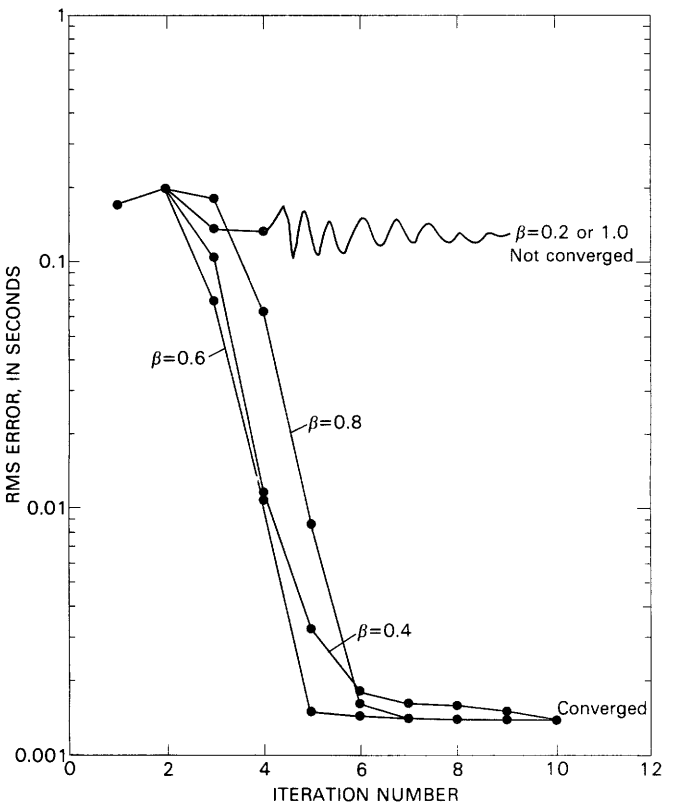

Figure 3. Graph showing the root-mean-square (RMS) error of inversion result when σ_t = 16 ms versus iteration number and various damping factors, β.

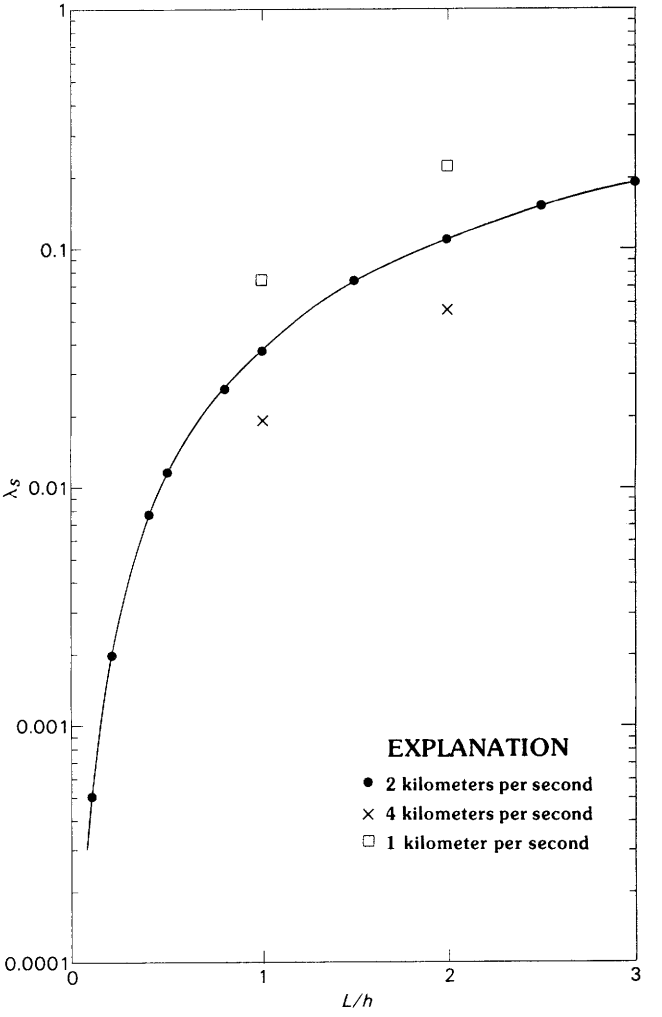

Figure 4. Graph showing smallest singular values of the Jacobian matrix (λ_s) in the singular value decomposition with respect to the ratio of spread length to target depth (*L*/*h*) for a one-layer model with the dip angle of 20°. Continuous line connecting dots is for velocity (*v*) = 2 km/s, squares for *v* = 1 km/s, and crosses for *v* = 4 km/s.

a biased solution. The regularization is closely related to the resolution of the solution and will be discussed later.

Using the initial estimates from table 1 and the geometry shown in figure 2*B*, with σ_t = 8 ms, inversion results for layer 7 produced parameter estimates of *v* = 3.49 km/s, ø = 1.81°, and *h* = 7.04 km when we dropped the solutions corresponding to λ_s less than 0.03. Compare this result to the estimation without regularization shown in table 3. The inversion result for layer 7 with regularization is very close to the true solution, but the inversion result incorporating regularization is highly dependent on the initial estimate: it provides a non-unique solution. When we use *h* = 8 km as an initial estimate instead of the 7 km shown in table 1, the inversion results with the same regularization are *v* = 5.11 km/s, ø = 5.68°, and *h* = 7.98 km. The standard deviation for layer 7 without regularization is the column vector of ($31\sigma_t$, $30\sigma_t$, $220\sigma_t$), and with regularization it is the column vector of ($0.08\sigma_t$, $1.11\sigma_t$, $0.14\sigma_t$). Hence, there is a significant reduction in the variance of the solution with regularization. As indicated by this example, the problem of regularization is the inconsistency of the solution. Thus, unless there is a good estimate of the initial parameters, it is difficult to apply regularization to the inversion problem. All of the inversion results for the models shown in the tables in this paper were estimated without regularization.

FIELD CONFIGURATION

In marine data acquisition, an off-end shooting geometry is always employed, but, in land data acquisition, either off-end or split-spread geometry may be used. In order to increase the accuracy of the interval velocity estimation using the stacking velocity, off-end geometry is sometimes used in a land survey, because, with the same group interval and number of channels, longer offsets can be obtained for velocity analysis.

In order to examine the effect of the offset distance on the traveltime inversion in the shot domain, the geometry shown in figure 5 is used. Figure 5 shows the ray paths for two off-end geometries and one split-spread geometry. The layer parameters for this model are identical to those shown in table 1 except for the first layer. Parameters for the first

Table 3. Comparison of inversion results using different random noise content

[Shooting geometry shown in figure 2. Random noise content, σ_t; group interval equals 200 meters; near-offset distance equals 152 meters; 20 channels]

Layer number	Velocity (kilometers per second) P-wave	Dip (degrees)	Depth (kilometers)
Random noise content (σ_t) = 4 milliseconds			
1	1.51	7.11	0.71
2	2.51	-4.95	1.30
3	3.84	-0.03	2.01
4	4.87	0.36	2.11
5	3.71	-9.69	2.99
6	4.30	16.16	5.05
7	4.23	-2.21	7.46
Random noise content (σ_t) = 8 milliseconds			
1	1.52	7.23	0.71
2	2.51	-4.90	1.30
3	3.88	-0.06	2.02
4	4.91	-0.73	2.12
5	3.64	-9.36	2.98
6	4.34	16.97	5.07
7	5.04	-5.31	7.94
Random noise content (σ_t) = 12 milliseconds			
1	1.52	7.35	0.72
2	2.52	-4.85	1.31
3	3.91	-0.09	2.03
4	4.91	1.10	2.13
5	3.55	-9.03	2.96
6	4.40	17.89	5.10
7	5.92	-8.76	8.49
Random noise content (σ_t) = 16 milliseconds			
1	1.53	7.46	0.72
2	2.52	-4.79	1.31
3	3.96	-0.12	2.04
4	4.86	1.44	2.14
5	3.46	-8.71	2.95
6	4.46	18.85	5.13
7	6.93	-13.01	9.13
Random noise content (σ_t) = 20 milliseconds			
1	1.54	7.58	0.73
2	2.53	-4.73	1.31
3	4.00	-0.15	2.05
4	4.80	1.74	2.15
5	3.38	-8.42	2.93
6	4.51	19.73	5.16
7	8.12	-18.70	9.97

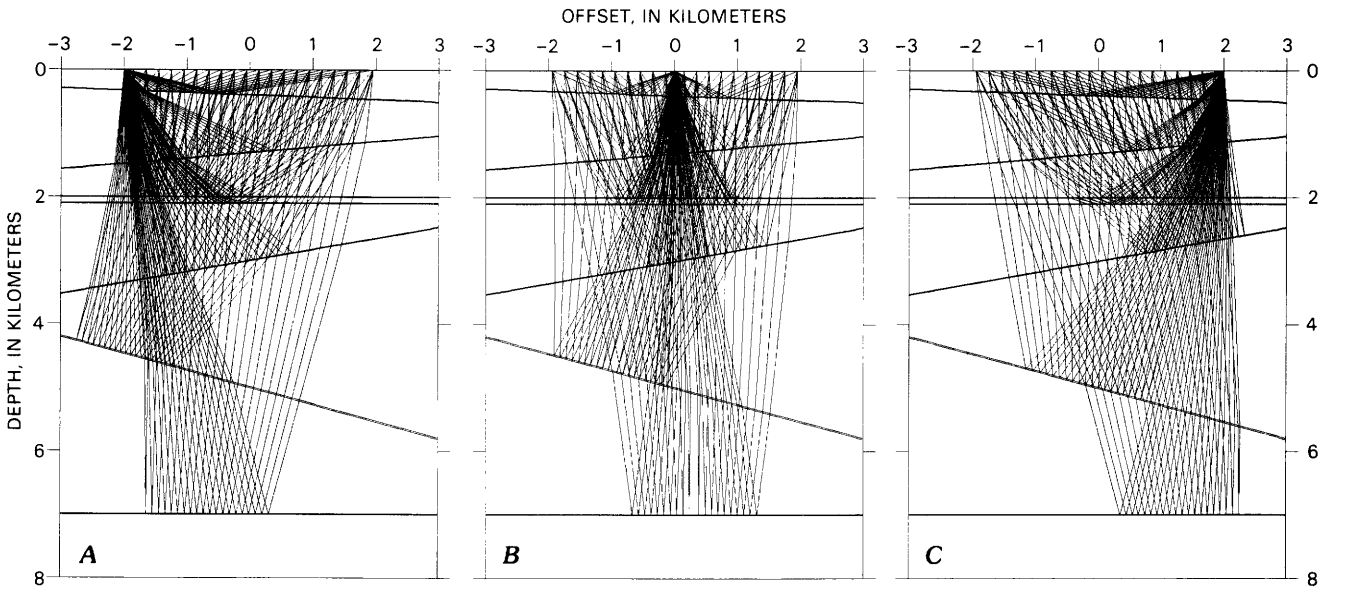

Figure 5. Ray tracings for shot gathers with geophone group interval of 0.2 km with 20 channels. Model parameters are identical to those shown in table 1 except for the first layer; parameters for the first layer are: velocity = 2 km/s, dip = 2°, and depth = 0.4 km. *A*, Off-end geometry with a source at –2 km; *B*, Split-spread geometry with a source at 0 km; *C*, Off-end geometry with a source at 2 km.

layer are: v = 2.0 km/s, ϕ = 2°, and h = 0.4 km. As can be seen in figure 5, identical group interval spacings and number of channels are employed. The far-offset distance for the off-end geometry is twice that of the split-spread configuration. The inversion results using the initial estimate shown in table 1 with σ_t = 8 ms are shown in table 4. The results shown in table 4 demonstrate that there is no apparent advantage for employing an off-end geometry in order to increase the offset distance. These results also indicate that split-spread geometry is better than off-end geometry for estimating dip angles.

In the case of horizontal layers, inversion results indicate that longer offset data are better for estimating layer parameters. Based on this model study, we conclude that the best way to increase the accuracy of inversion is to use the longest possible group intervals with a split-spread geometry for a given number of channels.

CMP DOMAIN INVERSION

The most common velocity analysis method in reflection seismology is performed in the CMP domain. Interval velocity can be computed by Dix's formula (Dix, 1955) if it is assumed that the stacking velocity is approximately equal to the RMS velocity. When dip angles are low and the offset distance is small compared to target depth, this method provides a reliable interval velocity estimate. The interval velocity may also be estimated in the CMP domain by the linear-inversion method.

In order to compare the shot domain inversion with the CMP domain inversion, the ray tracing for the CMP geometry based on model 1 was computed and the result shown in figure 6*A*. Figure 6*B* shows the CMP ray tracing result for model 1 with a low-velocity thin layer (v = 2.8 km/s) instead of a high-velocity layer (v = 4.8 km/s) for layer 4. In principle, we could include dip estimation in the CMP domain inversion process. However, our model study indicates that the inclusion of dip estimation hampers the convergence of the solution and produces a large variance for the estimated dip angle. The subsurface ray coverage for CMP geometry is very small (fig. 6) compared to the subsurface ray coverage for shot domain geometry (fig. 5). Thus, the estimation of dip angle using CMP geometry is not practical. Also, in the CMP domain, numerical simulation indicates that the smallest singular values for the inverse of the Jacobian matrix for model 1 is very small (on the order of 10^{-6}). Therefore, the best practical method for inverting CMP domain data requires estimating only interval velocities and depths. We can incorporate dip information from other sources, if available, into the inversion process.

The inversion results for the CMP domain data with the same geometry as shown in figure 6 are shown in table 5. When σ_t = 0, layer parameters were estimated within 4 percent. This error is introduced because of the horizontal layer assumption of the CMP domain inversion. In this example, where the maximum dip is on the order of 15°, the CMP domain inversion provided reliable layer parameters.

Table 4. Comparison of inversion results between split-spread and off-end shooting geometries

[Random noise content (σ_t) equals 8 milliseconds; group interval equals 200 meters; 20 channels]

Layer number	Velocity (kilometers per second) P-wave	Dip (degrees)	Depth (kilometers)
Off-end shooting source = –2.0 kilometers			
1	2.02	5.24	0.50
2	2.57	-4.76	1.33
3	3.97	0.41	2.07
4	4.89	0.65	2.17
5	3.47	-10.40	2.94
6	4.34	16.08	5.01
7	5.39	-3.8	8.19
Split-spread shooting source = 0 kilometers			
1	2.02	2.40	0.41
2	2.51	-4.91	1.30
3	3.89	-0.04	2.02
4	4.91	-0.72	2.12
5	3.60	-9.28	2.97
6	4.34	17.08	5.06
7	5.09	-5.42	7.96
Off-end shooting source = 2.0 kilometers			
1	2.02	-0.72	0.48
2	2.58	-5.98	1.35
3	3.99	-0.46	2.08
4	4.88	-0.61	2.18
5	3.74	-8.56	3.01
6	4.25	16.22	5.07
7	4.99	-7.83	8.00

Table 5 also contains the inversion result when measurement errors are introduced. Comparing these results with the shot domain inversion, it is obvious that the CMP domain inversion is not quite as sensitive to measurement noise. Particularly remarkable in this example is that the depth error of layer 7, even when $\sigma_t = 32$ ms, is less than a few percent. A comparison is also made in table 5 for the interval velocity estimates by a least-squares fitting of a hyperbola to the traveltime data and the Dix formula. The result for $\sigma_t = 16$ ms is shown in table 5 and shows that the result by CMP domain inversion is better than Dix's result for shallow reflections. This is possibly due to the hyperbolic assumption of traveltime. The interval velocity estimation by the Dix formula is also very insensitive to measurement noise.

The CMP domain inversion result for figure 6*B* shows that the layer parameters of the low-velocity thin layer have more error than those of the high-velocity thin layer. For example, when $\sigma_t = 16$ ms, the interval velocity is estimated to be 1.88 km/s, which is about a 33 percent error; thickness is estimated to be 60 m, which is 40 percent less than the true thickness. On the other hand, for the high-velocity layer, the velocity error is less than 4 percent and the thickness error is about 20 percent. When using Dix's formula for the low-velocity layer, the velocity is estimated to be 1.03 km/s, an error of more than 100 percent, and thickness is estimated to be less than 60 percent of the true thickness. This result is inferior to the CMP domain inversion result. However, in the shot domain, inversion errors for the thin layer were similar to each other regardless of velocity. The reason for the greater error in low-velocity, thin-layer inversion can be understood by examining the ray-path diagram shown in figure 6. The rays are focused around the CMP point for the low-velocity layer (fig. 6*B*) while the rays spread out farther laterally for the high-velocity layer (fig. 6*A*). Therefore, the arrival time difference between near-offset and far-offset for the low-velocity thin bed is much smaller than that for the high-

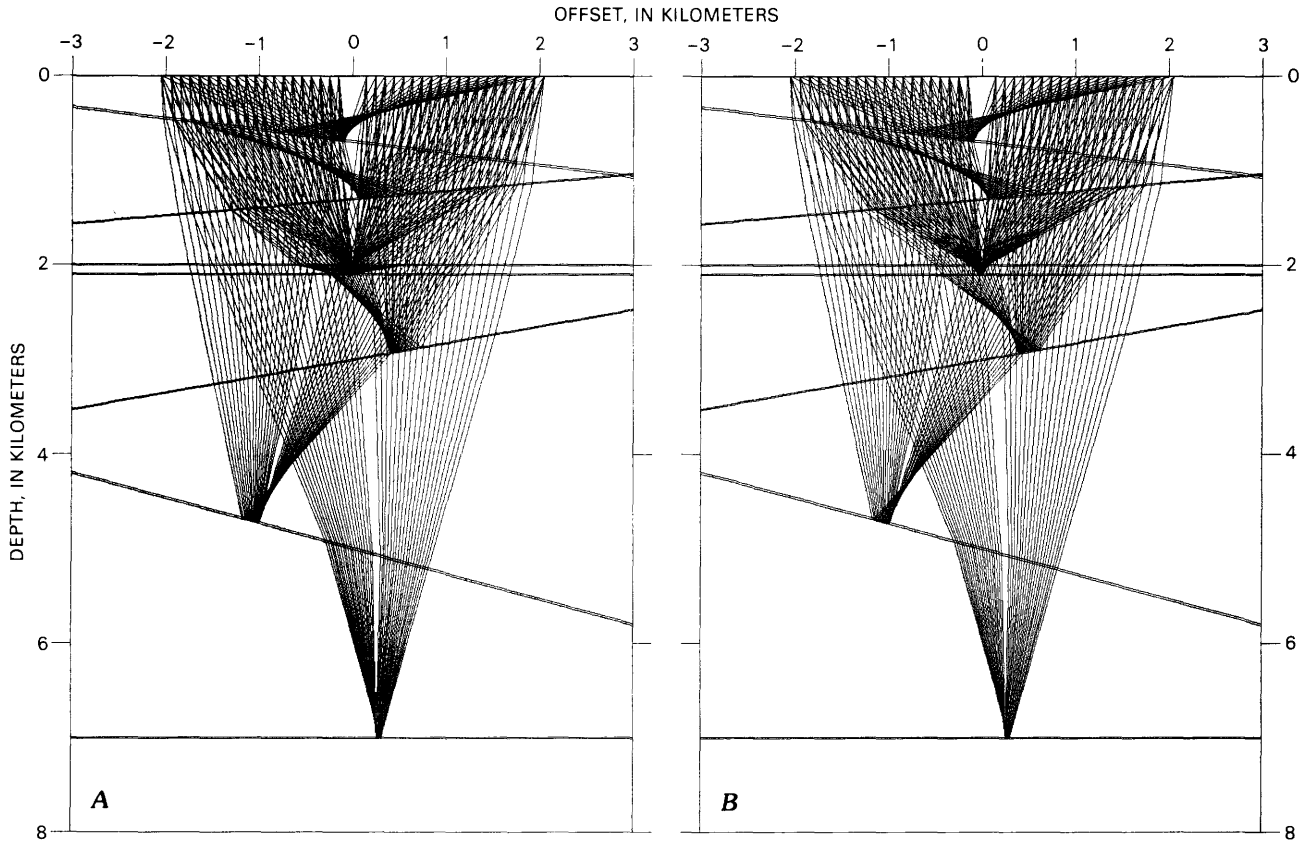

Figure 6. Ray tracings for common midpoint (CMP) gathers for CMP domain inversion. The CMP interval is 0.1 km, and model parameters are shown in table 1. *A*, High-velocity thin layer (velocity (v) = 4.8 km/s); *B*, Low-velocity thin layer (v = 2.8 km/s).

velocity thin bed. In fact, the arrival time difference is 178 ms for the low-velocity layer and 532 ms for the high-velocity layer. Thus, it may be more difficult to resolve the parameters of the low-velocity thin layer using CMP domain geometry.

MODE CONVERSION

Traveltime inversion including mode conversion at the reflecting boundary can be easily implemented using different velocities for the upgoing and downgoing ray paths. However, we cannot estimate all four layer-parameters (P-wave velocity, S-wave velocity, dip, and depth) simultaneously: we must know either the P-wave or S-wave velocity. This can be accomplished by first using P–P inversion (or S–S inversion), and then using the estimated P-wave (or S-wave) velocity to estimate other layer parameters using arrival times of the converted wave.

The ray-path diagram for the converted waves is shown in figure 7 using model 1. Figure 7*A* shows ray paths for the P–S converted waves and figure 7*B* shows ray paths for the S–P converted waves. The ray paths shown in figure 7 indicate that the rays of P–S converted waves spread out farther laterally than the S–P converted waves.

Inversion results for converted waves with σ_t = 8 ms are shown in table 6. Both estimated P-velocity (or S-velocity) using P–P inversion (or S–S inversion) and true velocity were used for comparison. Overall, there is no significant difference in the inversion result whether we use estimated or true velocity. Also, there is no significant difference in the inversion result between P–S and S–P converted waves. For layer 7, however, table 6 indicates that S–P data is slightly better than P–S data at estimating target depth. Because of the broad lateral coverage of rays from the P–S data shown in figure 7, intuition leads one to suspect that P–S data performs better than S–P data when estimating layer parameters. However, traveltime data show that the arrival time difference between near- and far-offsets is greater in S–P data than in P–S data. For this reason, the S–P data provides better results when estimating parameters of the deeper reflectors in this example.

These results demonstrate that the estimation of layer parameters using converted waves is feasible in principle. However, a multicomponent seismic data set using three-component geophones and different kinds of source polarization (Squire and others, 1988) is needed to utilize converted waves for traveltime inversion.

Table 5. Inversion results and Dix result for common midpoint shooting geometry and variable amounts of noise contamination

[Shooting geometry shown in figure 6. Common midpoint (CMP) interval equals 100 meters; 20 channels]

Layer number	Velocity (kilometers per second) P-wave	Dip (degrees)	Depth (kilometers)
Inversion result; random noise content (σ_t) = 0 milliseconds			
1	1.51	0.0	0.70
2	2.55	0.0	1.32
3	3.84	0.0	2.03
4	4.76	0.0	2.14
5	3.98	0.0	3.03
6	4.39	0.0	5.02
7	3.37	0.0	7.05
Inversion result; random noise content (σ_t) = 4 milliseconds			
1	1.51	0.0	0.70
2	2.54	0.0	1.32
3	3.84	0.0	2.03
4	4.76	0.0	2.12
5	4.00	0.0	3.03
6	4.34	0.0	5.00
7	3.37	0.0	7.03
Inversion result; random noise content (σ_t) = 16 milliseconds			
1	1.51	0.0	0.69
2	2.53	0.0	1.31
3	3.84	0.0	2.02
4	4.65	0.0	2.10
5	4.02	0.0	3.03
6	4.19	0.0	4.92
7	3.38	0.0	7.01
Inversion result; random noise content (σ_t) = 32 milliseconds			
1	1.50	0.0	0.68
2	2.52	0.0	1.30
3	3.83	0.0	2.01
4	3.83	0.0	2.07
5	4.08	0.0	3.02
6	4.00	0.0	4.82
7	3.39	0.0	6.86
Dix result; random noise content (σ_t) = 16 milliseconds			
1	1.51	0.0	0.70
2	2.77	0.0	1.39
3	4.10	0.0	2.13
4	4.88	0.0	2.22
5	3.90	0.0	3.10
6	4.15	0.0	4.97
7	3.37	0.0	7.00

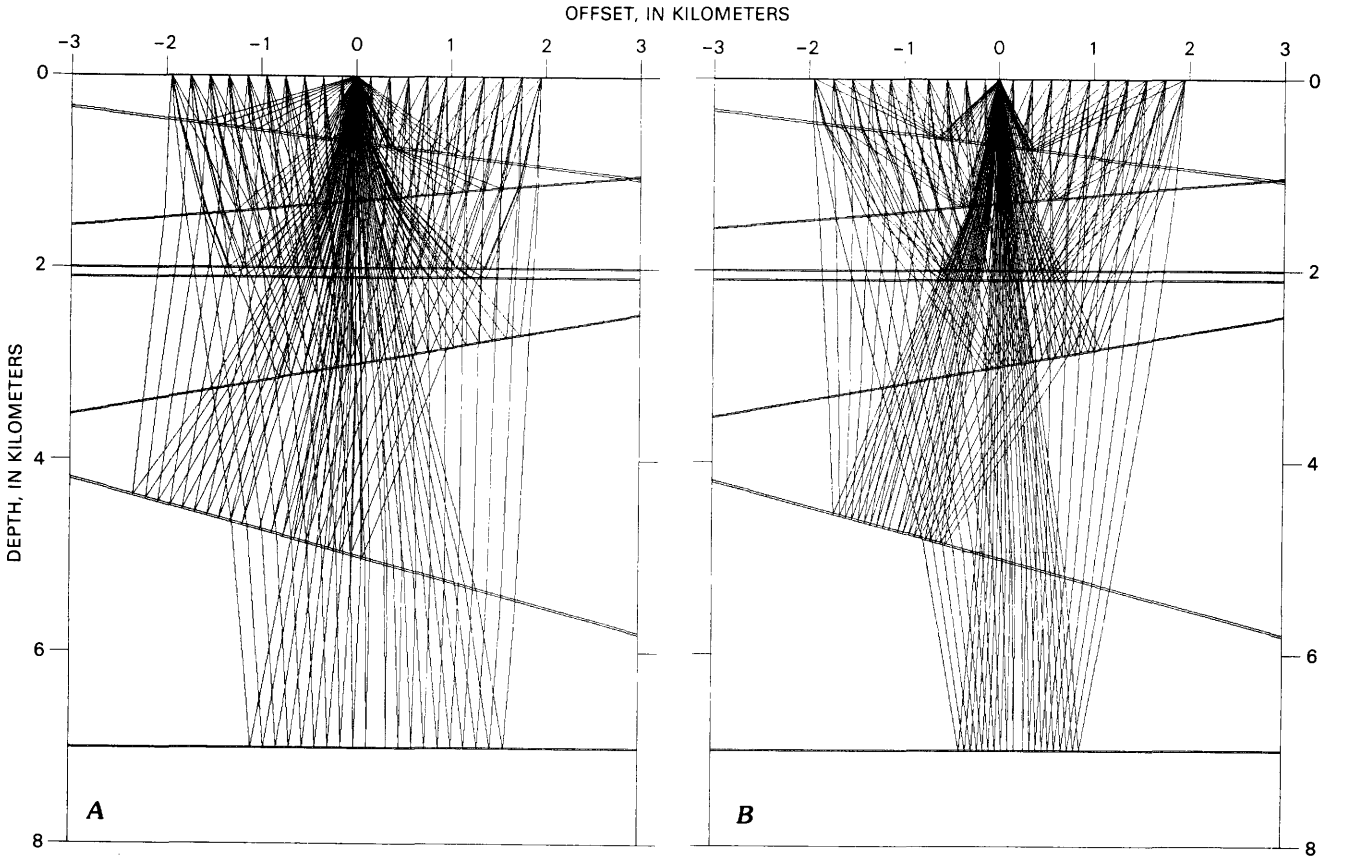

Figure 7. Ray tracings for shot domain inversion including mode conversion at the reflecting boundary. The geophone group interval is 0.2 km, and model parameters are shown in table 1. *A*, Longitudinal-shear (P–S) conversion; *B*, Shear-longitudinal (S–P) conversion.

REAL DATA EXAMPLES

In an attempt to apply the IWI inversion method to a real data set, a shot and CMP gather using real marine seismic data were used.

Figure 8*A* shows the observed arrival times (squares) and the computed arrival times (crosses) based on the shot domain inversion results shown in table 7. The RMS error between the observed and computed arrival times is about 1.6 ms. The corresponding ray-path diagram (not shown) for the inversion results indicates that there are crossing layers within the ray paths (layers 2 and 3 cross at a depth of about 1.5 km). Currently, the inversion program cannot handle crossing layers within a ray path. Therefore, offsets greater than 1.85 km were omitted for the deeper layer(s).

The results produced by CMP domain inversion are shown in figure 8*B* and table 7. The RMS error between observed and computed arrival times is about 2.2 ms. Also included are the results by fitting the arrival times by a hyperbola using the least squares method (table 7, fig. 8*C*); the RMS error between observed and computed arrival times is about 3.7 ms. This large RMS error was introduced by the mismatch between computed and measured arrival times at farther offsets. Notice that the computed arrival times are systematically earlier for the far offsets of layer 5 in figure 8*C*.

The inversion result in the CMP domain is very similar to the conventional method based on hyperbolic moveout even though a slight advantage of the inversion method can be justified based on figures 8*B* and 8*C*.

Shot domain and CMP domain results varied greatly. During the inversion of the CMP gather, the process converged to consistent estimates over wide ranges of initial conditions, regularization, and β's (see equation 10), while shot domain inversion provided many inconsistent results. For example, in the range of RMS error = 1.7 ms, the velocity of the second layer was estimated by shot domain inversion at 0.74 km/s with different regularization.

The problem in the shot domain inversion was in the second layer. The resolution matrix (see appendix A) of the second layer for the result shown for the shot domain inversion in table 7 is:

$$\begin{bmatrix} R_{ss} & R_{sa} & R_{sh} \\ R_{sa} & R_{aa} & R_{ah} \\ R_{sh} & R_{ah} & R_{hh} \end{bmatrix} = \begin{bmatrix} 0.02 & 0.08 & 0.11 \\ 0.08 & 0.99 & 0.0 \\ 0.11 & 0.0 & 0.99 \end{bmatrix}$$

Table 6. Inversion results including mode conversions for split-spread shooting geometry

[Shooting geometry shown in figure 7. Group interval equals 200 meters; near-offset distance equals 152 meters; 20 channels]

Layer number	Velocity (kilometers per second) P-wave	S-wave	Dip (degrees)	Depth (kilometers)
P–S conversion used estimated P-wave velocity				
1	1.52	1.00	7.10	0.71
2	2.51	1.25	-4.89	1.30
3	3.88	1.92	0.03	2.01
4	4.91	2.57	0.41	2.12
5	3.63	1.94	-9.50	2.98
6	4.34	1.96	16.49	5.06
7	5.04	2.00	-5.31	7.67
P–S conversion used true P-wave velocity				
1	1.50	1.02	7.32	0.71
2	2.50	1.26	-4.87	1.31
3	3.80	1.97	0.22	2.03
4	4.80	2.65	0.61	2.13
5	3.80	1.87	-9.19	2.98
6	4.20	1.93	16.43	5.03
7	3.50	2.40	-4.38	7.62
S–P conversion used estimated S-wave velocity				
1	1.52	1.01	7.25	0.71
2	2.51	1.25	-4.85	1.31
3	3.85	1.92	-0.16	2.01
4	4.98	2.54	-0.70	2.12
5	3.64	1.95	-9.55	2.98
6	4.31	1.94	16.59	5.05
7	4.90	1.94	-3.53	7.57
S–P conversion used true S-wave velocity				
1	1.52	1.00	7.35	0.71
2	2.51	1.25	-4.94	1.30
3	3.88	1.90	0.13	2.01
4	5.03	2.50	0.73	2.11
5	3.58	2.00	-9.59	2.99
6	4.29	1.90	16.28	5.02
7	5.52	1.60	-2.77	7.28

As mentioned by Tarantola (1987) and Jackson (1972), the resolution matrix of well-resolved parameters is close to the identity matrix. The resolution matrix of layer 2 has a very low number for the slowness. This means that we may not resolve the velocity of the second layer with the current data set and the assumptions of our current model (i.e., assuming that the earth's crust consists of iso-velocity layers separated by plane interfaces).

Although dip directions estimated by shot domain inversions are consistent with the seismic data, this example shows that shot domain inversion has many difficulties.

As mentioned earlier, the main advantage of shot domain inversion over the CMP domain inversion is its ability to estimate dips. Both shot domain and CMP domain inversion were applied to a 1024-channel sign-bit data set. The migrated portion of the line is shown in figure 9, and the inversion analysis was done in the vicinity of CMP 1650. The measured arrival times are shown as squares and the computed arrival times are shown as crosses in figure 10. The average RMS error between observed and computed arrival times was 14 ms; most of the errors occurred at layer 6.

Table 7. Comparison of inversion results using real marine seismic data

[RMS, root-mean-square; CMP, common midpoint]

Layer number	Velocity (kilometers per second) P-wave	Dip (degrees)	Depth (kilometers)
Shot domain inversion; RMS error = 1.6 milliseconds			
1	1.47	-3.34	
2	1.12	-3.00	0.73
3	1.80	-5.96	0.81
4	1.24	-6.44	1.01
5	2.40	0.86	1.55
CMP domain inversion; RMS error = 2.2 milliseconds			
1	1.52	0.0	0.62
2	1.21	0.0	0.74
3	2.06	0.0	0.80
4	1.66	0.0	1.08
5	2.43	0.0	1.65
CMP domain hyperbolic fitting; RMS error = 3.7 milliseconds			
1	1.51	0.0	0.61
2	1.22	0.0	0.74
3	2.19	0.0	0.81
4	1.64	0.0	1.08
5	2.50	0.0	1.68

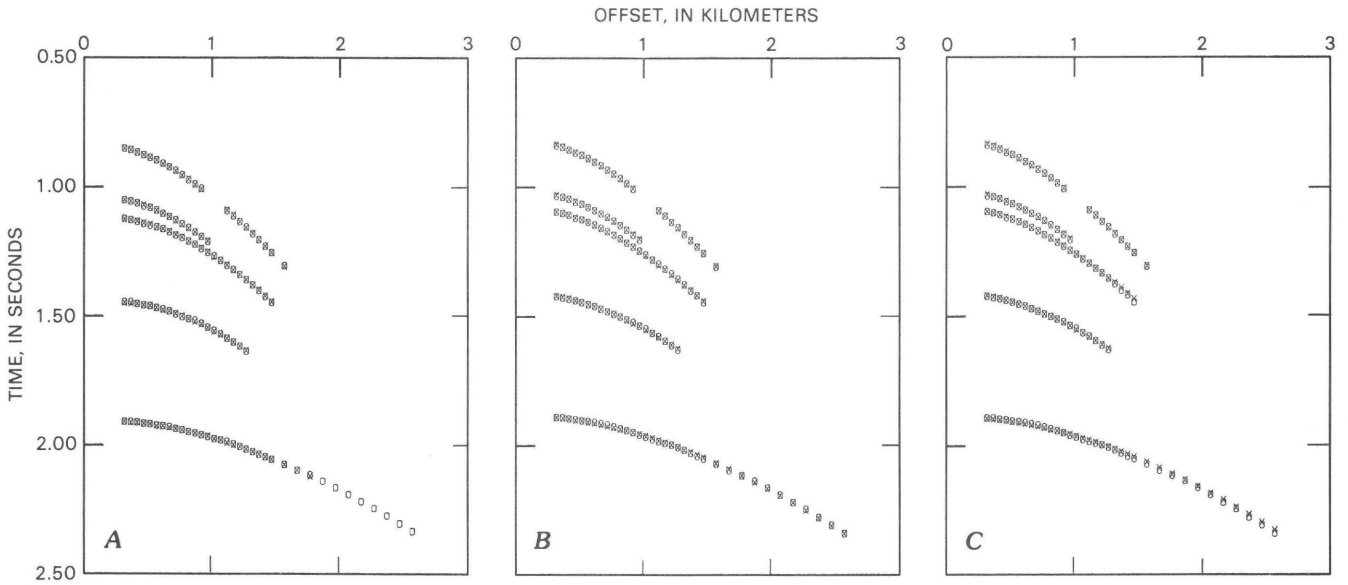

Figure 8. Graphs showing measured and computed arrival times for marine multichannel data. Squares indicate measured arrival times and crosses indicate estimated arrival times. *A*, Shot domain inversion results with root-mean-square (RMS) error of 1.6 ms; *B*, Common midpoint (CMP) domain inversion results with RMS error of 2.2 ms; *C*, Interval velocity estimated assuming hyperbolic moveout times and Dix's formula with RMS error of 3.7 ms.

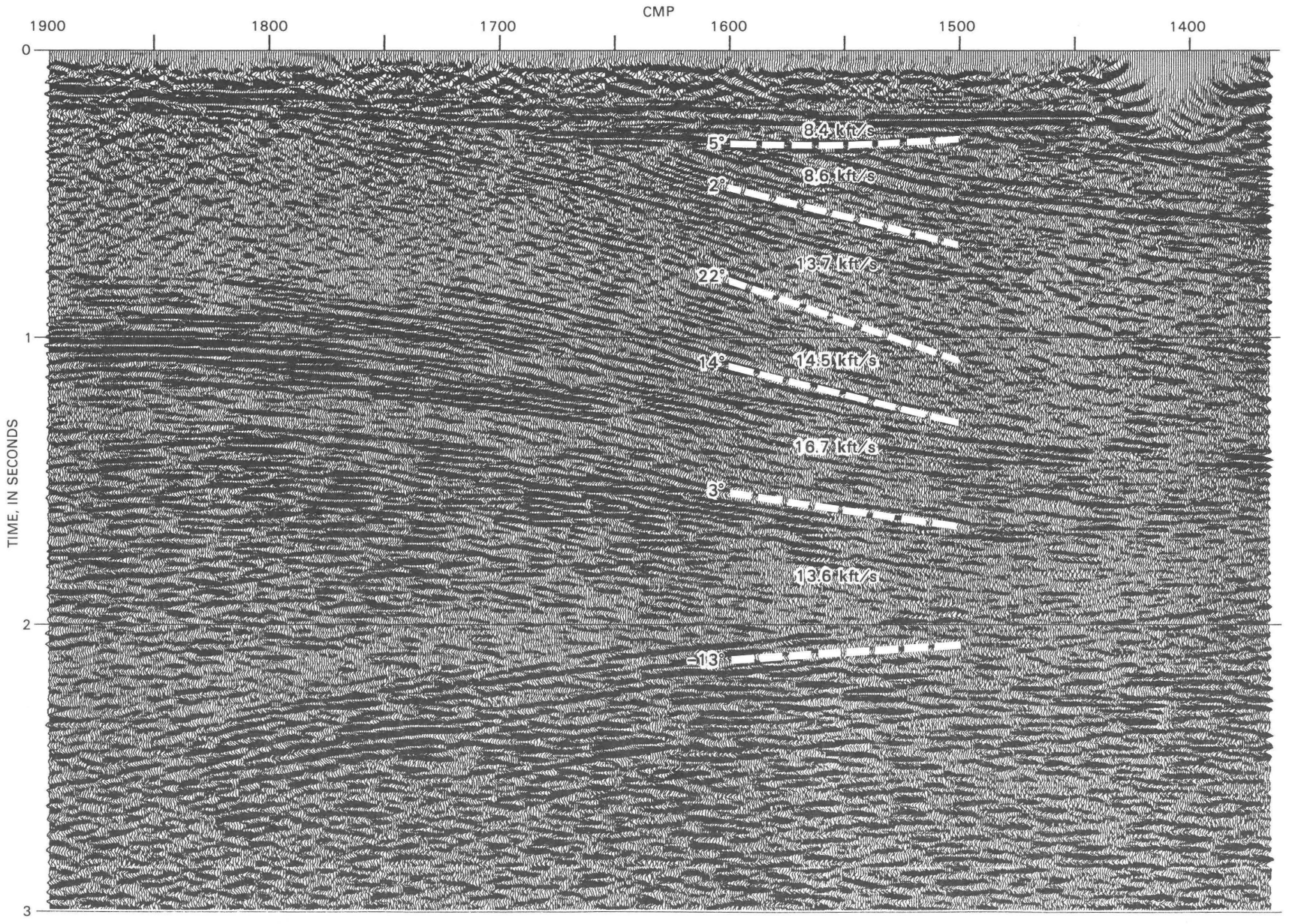

Figure 9. Migrated stacked section of sign-bit data. Estimated interval velocities and dips by a shot domain inversion are shown near common midpoint (CMP) 1650.

The overall dips of the inversion result of a single shot agree well with the migrated section except for layer 2. The dip of layer 2 in the migrated section is similar to the dip of layer 3, but the inversion result indicates negligible dip for layer 2. This is possibly due to the error in picking arrival times for the inversion. The interval velocity based on the stacking velocity is about 40 to 60 percent higher than the inversion result shown in figure 9. However, the migration velocity analysis agrees well with the inversion result.

DISCUSSION

We have described a linear traveltime inversion method which is computationally efficient and accurate. This computational method was derived by suitable estimation of model parameters in such a way that the Jacobian matrix is in a lower triangular form. However, the application of this method to real data suggests some problems.

The chief problem may be caused by the iso-velocity and plane-layer assumptions in our crustal model. Particularly in the shot domain, estimation of dip angle is closely related to other layer parameters such as velocity and depth. The elements of the correlation coefficient matrix (Tarantola, 1987) are close to 1.0: this indicates that the error in one parameter estimate will always affect the other layer parameters. Numerous tests on models and real data indicate that the dip angle is most difficult to handle in the shot domain inversion. With a given field geometry, slight changes in dip angles significantly change the other layer parameters.

In the shot domain, dip estimation may be affected significantly due to the lateral heterogeneity of the media. Thus, with real data, the result of the shot domain inversion frequently shows inconsistent estimates. In order to deal with this difficulty, we need a more complex model than the iso-velocity and plane-layer model considered in this paper. For the case of a more complex crustal model, the Jacobian matrix cannot be computed as shown in equation 7 but can be computed by a finite-difference method. The variable-mode velocity assumption by Zhu and Brown (1987) is one way of introducing lateral heterogeneity. Even in this case, the iterative whole-layer inversion method described here can be implemented by the parameterization shown in this paper.

In the CMP domain, because we ignored dip angle during inversion, the estimated layer parameters were more consistent than the layer parameters estimated in the shot domain. As mentioned by Diebold and Stoffa (1981), the CMP domain inversion averages out lateral heterogeneity, and, as a consequence, the iso-velocity assumption seems to work better in this domain. If we want to investigate a detailed velocity structure of the lower crust where the two-way traveltime is in the range of 5 to 10 s, an expanding-spread geometry could have an advantage over a long-offset shot gather.

Problems may arise in picking arrival times in the shot domain. The error in dip estimation for layer 2, using the sign-bit data shown in figure 9, was caused by picking a crossing event. The original data showed many crossing events in the upper part of the section making it difficult to identify true reflections. In cases where there is much coherent noise, extensive shot domain pre-processing is necessary. Therefore, in such cases, implementing conventional velocity analysis based on hyperbolic moveout is much easier.

The RMS error between observed and computed arrival times serves as an indicator of convergence. However, because of the non-uniqueness of the inversion, sound geological judgment should be employed when interpreting inversion results. As indicated in the model study, convergence depends on the initial estimate as well as on the inversion method used. For example, the RMS error of one of the inversion results for the sign-bit data shown in figure 10 was 7.3 ms, which is about one-half of the RMS error of the result shown in figure 9. The inversion result with an RMS error of 7.3 ms was identical to the result shown in figure 9 except for layer 6. The velocity of layer 6 was estimated as 9.8 kft/s (kilofeet per second) with an 8° dip. Both inversion results reveal a low-velocity zone for layer 6. Based on a priori geologic knowledge of the area, we chose the 13.5 kft/s velocity layer over the 9.8 kft/s layer even though it had a higher RMS error value. In this example, because we do not have other independent sources of velocity information such as well logs, we are not sure which value is closer to the true interval velocity.

CONCLUSIONS

Based on model analysis and real data examples, the following conclusions can be drawn:

1. The iterative whole-layer inversion method is superior to the layer-stripping method for estimating layer parameters such as velocity, dip, and depth in the shot domain. However, in the CMP domain, the two methods yield similar results.
2. A split-spread geometry gives better results than off-end geometry for the shot domain inversion, particularly for dip estimation.
3. CMP domain inversion is less sensitive to measurement noise compared to shot domain inversion.
4. In order to calculate a reliable layer parameter, the surface-spread length should approximately equal the target depth of interest.

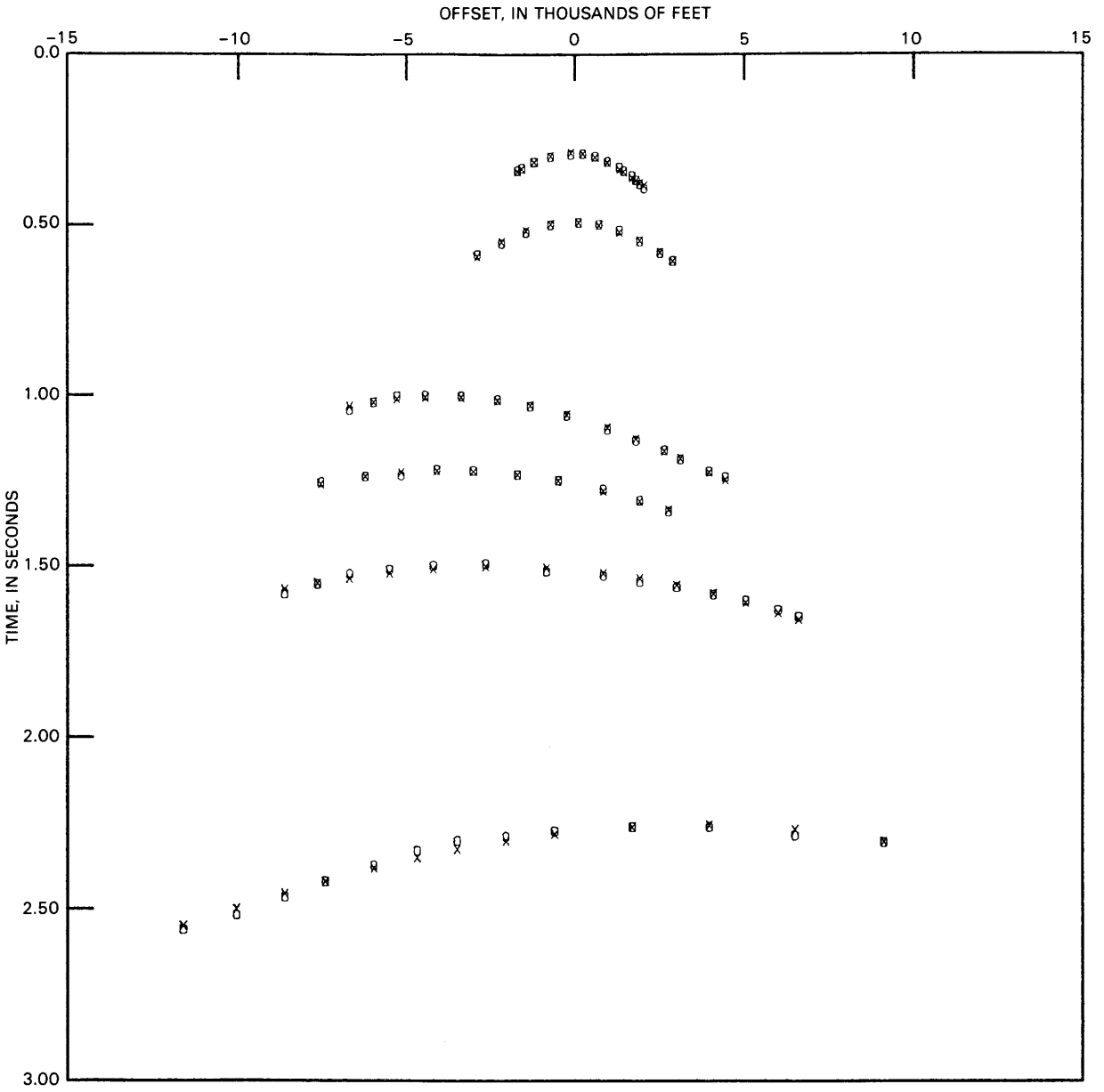

Figure 10. Graph of measured arrival times (squares) and computed arrival times (crosses) resulting from a shot domain inversion near common midpoint (CMP) 1650 in figure 9. The root-mean-square (RMS) error of inversion is about 14 ms.

5. Regularization is a good method of reducing the variance of layer parameters, but, owing to the inconsistency of the solution, care should be taken when implementing regularization.
6. CMP domain inversion has an advantage over conventional velocity analysis based on hyperbolic moveout for longer offset data. The conventional method has an advantage in implementation because it does not require the digitization of arrival times.
7. The inversion of converted waves may be feasible using a real data set.

APPENDIX A

Resolution Matrix

The resolution matrix $\boldsymbol{R}$ can be defined in a singular value decomposition of the Jacobian matrix (equation 4) by the following formula (Jackson, 1972):

$$\boldsymbol{R} = \boldsymbol{V}\boldsymbol{V}^t$$

Because V is an orthonormal eigenvector, R is the identity matrix (I). In the case when solutions corresponding to smaller singular values are eliminated in order to reduce the variance of the solution, the resolution matrix can be written as:

$$R_{ij} = \sum_{k=1}^{q} V_{ik} V_{jk} \qquad \text{(A1)}$$

where

q represents the number of singular values kept for the solution.

The resolution matrix given in the main text was evaluated using equation A1 with $q = 2$.

The physical meaning of the resolution matrix can be illustrated by a formula given by Tarantola (1987). He presented the following formula for the resolution matrix:

$$\langle M \rangle = R\,(M_t - M_p) + M_p \qquad \text{(A2)}$$

where

$\langle M \rangle$ is the inverse solution of model parameters,
M_t is the true model parameter, and
M_p is the prior model parameter.

Equation A2 indicates that we are able to see the truth only through a filter R. In a favorable case, $R \approx I$.
Thus,

$$\langle M \rangle \approx M_t$$

The more R differs from the identity matrix, the more the estimation differs from the true model parameters.

REFERENCES CITED

Aki, K., and Lee, W.H.K., 1976, Determination of three-dimensional velocity anomalies under a seismic array using first P arrival times from local earthquakes; 1, A homogeneous initial model: Journal of Geophysical Research, v. 81, no. 23, p. 4381–4399.

Aki, K., and Richards, P.G., 1980, Quantitative seismology—theory and methods, 2: San Francisco, W.H. Freeman, 932 p.

Backus, G., and Gilbert, F., 1970, Uniqueness in the inversion of inaccurate gross Earth data: Philosophical Transactions of the Royal Society of London, v. 266, no. 1173, p. 123–192.

Bishop, T.N., Bube, K.P., Cutler, R.T., Lanegan, R.T., Love, P.L., Resnick, J.R., Shuey, R.T., Spindler, D.A., and Wyld, H.W., 1985, Tomographic determination of velocity and depth in laterally varying media: Geophysics, v. 50, no. 6, p. 903–923.

Chiu, S.K.L., and Stewart, D.R., 1987, Tomographic determination of three-dimensional seismic velocity structure using well logs, vertical seismic profiles, and surface seismic data: Geophysics, v. 52, no. 8, p. 1085–1098.

Diebold, J.B., and Stoffa, P.L., 1981, The traveltime equation, tau-p mapping, and inversion of common midpoint data: Geophysics, v. 46, no. 3, p. 238–254.

Diebold, J.B., Stoffa, P.L., and the LASE study group, 1988, A large aperture seismic experiment in the Baltimore Canyon trough *in* Sheridan, R.E., and Grow, J.A., eds., The Atlantic continental margin; U.S., The geology of North America, v. 1–2: The Geological Society of America, p. 387–398.

Dix, C.H., 1955, Seismic velocity from surface measurements: Geophysics, v. 20, no. 1, p. 68–86.

Gjøystdal, Håvar, and Ursin, Bjørn, 1981, Inversion of reflection times in three dimensions: Geophysics, v. 46, no. 7, p. 972–983.

Jackson, D.D., 1972, Interpretation of inaccurate, insufficient, and inconsistent data: Geophysical Journal of the Royal Astronomical Society, v. 28, p. 97–109.

Lee, M.W., 1990, Traveltime inversion using transmitted waves of offset VSP data: Geophysics, v. 55, no. 8, p. 1089–1097.

Lines, L.R., ed., 1988, Inversion of geophysical data: Geophysics reprint series 9, Society of Exploration Geophysicists, 543 p.

Lines, L.R., Bourgeois, A., and Covey, J.D., 1984, Traveltime inversion of offset vertical seismic profiles—a feasibility study: Geophysics, v. 49, no. 3, p. 250–264.

Lines, L.R., and Treitel, S., 1984, Tutorial: A review of least-squares inversion and its application to geophysical problems: Geophysical Prospecting, v. 32, no. 2, p. 159–186.

Liu, Char-Shine; Zhu, Tianfei; Farmer, Harlow; and Brown, Larry, 1986, An expanding-spread experiment during COCORP's field operation in Utah, *in* Barazangi, M., and Brown, L., eds., Reflection seismology: A global perspective: American Geophysical Union, Geodynamics Series, v. 13, p. 237–246.

Sluis, A. van der, and Vorst, H.A. van der, 1987, Numerical solution of large, sparse linear algebraic systems arising from tomographic problems *in* Nolet, G., ed., Seismic tomography with applications in global seismology and exploration geophysics: Dordrecht, D. Reidel Publishing Company, p. 49–83.

Squire, S.G., Kim, C.D.Y., and Kim, D.Y., 1988, Interpretation of total wave field data over Last Hills Fields, Kern County, California: 58th Annual International Meeting of Society of Exploration Geophysicists, Expanded Abstracts, p. 1137–1141.

Tarantola, A.T., 1987, Inverse problem theory: Amsterdam, Elsevier, 613 p.

Zhu, T., and Brown, L.D., 1987, Two-dimensional velocity inversion and synthetic seismogram computation: Geophysics, v. 52, no. 1, p. 37–50.

☆U.S. GOVERNMENT PRINTING OFFICE: 1991-573-049/46004

SELECTED SERIES OF U.S. GEOLOGICAL SURVEY PUBLICATIONS

Periodicals

Earthquakes & Volcanoes (issued bimonthly).
Preliminary Determination of Epicenters (issued monthly).

Technical Books and Reports

Professional Papers are mainly comprehensive scientific reports of wide and lasting interest and importance to professional scientists and engineers. Included are reports on the results of resource studies and of topographic, hydrologic, and geologic investigations. They also include collections of related papers addressing different aspects of a single scientific topic.

Bulletins contain significant data and interpretations that are of lasting scientific interest but are generally more limited in scope or geographic coverage than Professional Papers. They include the results of resource studies and of geologic and topographic investigations; as well as collections of short papers related to a specific topic.

Water-Supply Papers are comprehensive reports that present significant interpretive results of hydrologic investigations of wide interest to professional geologists, hydrologists, and engineers. The series covers investigations in all phases of hydrology, including hydrogeology, availability of water, quality of water, and use of water.

Circulars present administrative information or important scientific information of wide popular interest in a format designed for distribution at no cost to the public. Information is usually of short-term interest.

Water-Resources Investigations Reports are papers of an interpretive nature made available to the public outside the formal USGS publications series. Copies are reproduced on request unlike formal USGS publications, and they are also available for public inspection at depositories indicated in USGS catalogs.

Open-File Reports include unpublished manuscript reports, maps, and other material that are made available for public consultation at depositories. They are a nonpermanent form of publication that may be cited in other publications as sources of information.

Maps

Geologic Quadrangle Maps are multicolor geologic maps on topographic bases in 7 1/2- or 15-minute quadrangle formats (scales mainly 1:24,000 or 1:62,500) showing bedrock, surficial, or engineering geology. Maps generally include brief texts; some maps include structure and columnar sections only.

Geophysical Investigations Maps are on topographic or planimetric bases at various scales; they show results of surveys using geophysical techniques, such as gravity, magnetic, seismic, or radioactivity, which reflect subsurface structures that are of economic or geologic significance. Many maps include correlations with the geology.

Miscellaneous Investigations Series Maps are on planimetric or topographic bases of regular and irregular areas at various scales; they present a wide variety of format and subject matter. The series also includes 7 1/2-minute quadrangle photogeologic maps on planimetric bases which show geology as interpreted from aerial photographs. Series also includes maps of Mars and the Moon.

Coal Investigations Maps are geologic maps on topographic or planimetric bases at various scales showing bedrock or surficial geology, stratigraphy, and structural relations in certain coal-resource areas.

Oil and Gas Investigations Charts show stratigraphic information for certain oil and gas fields and other areas having petroleum potential.

Miscellaneous Field Studies Maps are multicolor or black-and-white maps on topographic or planimetric bases on quadrangle or irregular areas at various scales. Pre-1971 maps show bedrock geology in relation to specific mining or mineral-deposit problems; post-1971 maps are primarily black-and-white maps on various subjects such as environmental studies or wilderness mineral investigations.

Hydrologic Investigations Atlases are multicolored or black-and-white maps on topographic or planimetric bases presenting a wide range of geohydrologic data of both regular and irregular areas; principal scale is 1:24,000 and regional studies are at 1:250,000 scale or smaller.

Catalogs

Permanent catalogs, as well as some others, giving comprehensive listings of U.S. Geological Survey publications are available under the conditions indicated below from the U.S. Geological Survey, Books and Open-File Reports Section, Federal Center, Box 25425, Denver, CO 80225. (See latest Price and Availability List.)

"Publications of the Geological Survey, 1879- 1961" may be purchased by mail and over the counter in paperback book form and as a set of microfiche.

"Publications of the Geological Survey, 1962- 1970" may be purchased by mail and over the counter in paperback book form and as a set of microfiche.

"Publications of the U.S. Geological Survey, 1971- 1981" may be purchased by mail and over the counter in paperback book form (two volumes, publications listing and index) and as a set of microfiche.

Supplements for 1982, 1983, 1984, 1985, 1986, and for subsequent years since the last permanent catalog may be purchased by mail and over the counter in paperback book form.

State catalogs, "List of U.S. Geological Survey Geologic and Water-Supply Reports and Maps For (State)," may be purchased by mail and over the counter in paperback booklet form only

"Price and Availability List of U.S. Geological Survey Publications," issued annually, is available free of charge in paperback booklet form only.

Selected copies of a monthly catalog "New Publications of the U.S. Geological Survey" available free of charge by mail or may be obtained over the counter in paperback booklet form only. Those wishing a free subscription to the monthly catalog "New Publications of the U.S. Geological Survey" should write to the U.S. Geological Survey, 582 National Center, Reston, VA 22092.

Note.--Prices of Government publications listed in older catalogs, announcements, and publications may be incorrect. Therefore, the prices charged may differ from the prices in catalogs, announcements, and publications.